INTERNATIONAL JOURNAL FOR NUMERICAL METHODS IN FLUIDS
Int. J. Numer. Meth. Fluids 2009; **59**:1051–1062
Published online 30 July 2008 in Wiley InterScience (www.interscience.wiley.com). DOI: 10.1002/fld.1864

An implementation of the Spalart–Allmaras DES model in an implicit unstructured hybrid finite volume/element solver for incompressible turbulent flow

Shuangzhang Tu, Shahrouz Aliabadi*, †, Reena Patel and Marvin Watts

Northrop Grumman Center for HPC of Ship Systems Engineering, Jackson State University, Jackson, MS 39204, U.S.A.

SUMMARY

In this paper, we describe an implicit hybrid finite volume (FV)/element (FE) incompressible Navier–Stokes solver for turbulent flows based on the Spalart–Allmaras detached eddy simulation (SA-DES). The hybrid FV/FE solver is based on the segregated pressure correction or projection method. The intermediate velocity field is first obtained by solving the original momentum equations with the matrix-free implicit cell-centered FV method. The pressure Poisson equation is solved by the node-based Galerkin FE method for an auxiliary variable. The auxiliary variable is closely related to the real pressure and is used to update the velocity field and the pressure field. We store the velocity components at cell centers and the auxiliary variable at vertices, making the current solver a staggered-mesh scheme. The SA-DES turbulence equation is solved after the velocity and the pressure fields have been updated at the end of each time step. The same matrix-free FV method as the one used for momentum equations is used to solve the turbulence equation. The turbulence equation provides the eddy viscosity, which is added to the molecular viscosity when solving the momentum equation. In our implementation, we focus on the accuracy, efficiency and robustness of the SA-DES model in a hybrid flow solver. This paper will address important implementation issues for high-Reynolds number flows where highly stretched elements are typically used. In addition, some aspects of implementing the SA-DES model will be described to ensure the robustness of the turbulence model. Several numerical examples including a turbulent flow past a flat plate and a high-Reynolds number flow around a high angle-of-attack NACA0015 airfoil will be presented to demonstrate the accuracy and efficiency of our current implementation. Copyright © 2008 John Wiley & Sons, Ltd.

Received 3 October 2007; Revised 9 May 2008; Accepted 25 May 2008

KEY WORDS: incompressible flows; hybrid finite volume/element method; high Reynolds number flow; turbulent flow

*Correspondence to: Shahrouz Aliabadi, Northrop Grumman Center for HPC of Ship Systems Engineering, Jackson State University, Jackson, MS 39204, U.S.A.
†E-mail: saliabadi@jsums.edu

Contract/grant sponsor: Northrop Grumman Ship Systems
Contract/grant sponsor: National Science Foundation

1. INTRODUCTION

Recently, we developed a hybrid finite volume (FV)/element (FE) solver [1] for incompressible flows. The hybrid solver is based on the well-known pressure correction (projection) method [2, 3]. The solution procedure follows a segregated approach to decouple the pressure from the velocity. The velocity field is updated by solving the momentum equation provided that a known pressure field is given as a source term, through a cell-centered FV discretization. The pressure does not directly enter the momentum equation. Instead, an auxiliary variable, which is closely related to the pressure, takes the place of pressure in the momentum equation, providing pressure gradient information. We put the auxiliary variable on the vertices of cells. This deployment provides a convenient way to evaluate the pressure gradient using the local FE basis functions. The incremental value of the auxiliary variable is computed by solving a Poisson equation using the Galerkin finite element method. The auxiliary variable is then used to update the velocity field. After the final velocity field is determined, the pressure can be updated using the auxiliary variable and the velocity divergence field. The pressure is updated in such a way that the pressure field is free of unphysical conditions in the boundary layer.

Our hybrid FV/FE solver is aimed to take advantage of the merits of both the FV and the FE methods and avoid their shortcomings. For example, highly stretched cells (also known as high-aspect-ratio cells) are commonly used inside the boundary layer for high Reynolds number flows to resolve the boundary layer and reduce the number of cells. The stabilization parameters in the stabilized FE-based flow solvers [4, 5] are related to the characteristic element length, which is not well defined for high-aspect-ratio mesh elements. Owing to this, it is very difficult to control the numerical dissipation of stabilized FE solvers. By contrast, the FV flow solver is very insensitive to the aspect ratio of the mesh cells. It is quite common for the FV solvers to handle cells with aspect ratios in the order of thousands [6, 7]. For this reason, we use the FV method to solve the momentum equation. On the other hand, the classic Galerkin FE method is very suitable for the elliptic typed equations like the pressure Poisson equation emerging from the segregated approach. Therefore, the combination of the FV method and the FE method is expected to perform well in the incompressible flow solvers based on the pressure project method, which has been confirmed by our earlier work [1].

Our hybrid solver has been demonstrated to possess such features as (1) free of velocity–pressure odd–even decoupling phenomenon, (2) correct temporal convergence rates for both velocity and pressure, (3) free of unphysical pressure boundary layer, (4) good convergence in steady-state simulations and (5) capability in predicting accurate drag, lift and the Strouhal numbers [1]. The numerical examples we presented in [1] are all about low Reynolds number flows. When we tried to run the same code for high Reynolds number flows, we ran into the instability problem. After careful investigation, we found that the instability emerged first inside the boundary layer where highly stretched cells are used. Further investigation showed that the evaluation of the advection speed at cell interfaces in the FV solver is not dissipative enough to suppress the instability. Moreover, the mesh node may lie outside the convex hull formed by its surrounding cell centers when highly stretched cells are located in the region with large local wall surface curvature. When this happens, the solution at the vertex computed using the approach in [1] may not be within the range defined by the solutions at the vertex's neighboring cell centers. In return, the solution gradients inside the cell cannot be reliably reconstructed via the Gauss theorem, which utilizes the solution at vertices. In this paper, we will describe some remedies to improve the robustness of our hybrid solver for high Reynolds number flows.

DOI: 10.1002/fld

In addition to the high-aspect-ratio cell issue, we also need to incorporate an appropriate turbulence model into the flow solver to compute the eddy viscosity. This is essential to accurately predict the aerodynamic or hydrodynamic forces in high Reynolds number flows. However, the turbulence modeling is the least reliable aspect in the computational fluid dynamics simulations. Among the various turbulence modelings including the Reynolds-averaged Navier–Stokes (RANS) models, detached eddy simulation (DES), large eddy simulation (LES) and direct numerical simulation, the DES approach is the most practical and a fairly accurate turbulence model. The DES model was originally proposed [8] to be an affordable hybrid RANS/LES model for flows at realistic Reynolds numbers. In attached boundary layers, the DES model acts as a RANS model and in massively separated regions the DES functions as the LES model. A modified distance to the wall named the DES distance acts as a switch between the RANS mode and the LES mode. There are two DES-based turbulence modelings. One is the one-equation Spalart–Allmaras (SA) DES model [8, 9]. The other is the two-equation Shear Stress Transport DES model [10]. The SA-DES model is gaining more popularity [11–13] due to its simplicity and fair accuracy. In this paper, we incorporate the SA-DES turbulence model into our hybrid solver. The production and destruction terms in the SA-DES equation may cause overflows/underflows if not implemented properly. Therefore, we will address in this paper some implementation issues to ensure the robustness of the SA-DES model.

2. IMPLEMENTATION DETAILS FOR HIGH-ASPECT-RATIO CELLS

The details of our implicit hybrid FV/FE flow solver for incompressible flows are described in [1]. In this section, we address a couple of issues regarding how to ensure the robustness of the current hybrid solver for high Reynolds number flows. The purpose is to provide some remedies to cure the deficiency of our hybrid solver for high Reynolds number flows.

2.1. Solution at vertices

It is mentioned in [1] that we use the Gauss theorem to compute the velocity gradients inside each cell. The Gauss theorem states that for each component of the velocity $\mathbf{u}$, denoted by u, at cell i

$$\nabla u_i = \frac{1}{|\Omega_i|} \sum_{k=1}^{n_f} u_k A_k \mathbf{n}_k \tag{1}$$

where u_k is the interpolated solution at the κth face center. u_k is obtained by taking the arithmetic average of the interpolated solutions at the vertices. A_k and $\mathbf{n}_k$ are the area and outward unit normal of the κth face, respectively. Hence, the key is to obtain the solution at vertices accurately.

Since the solution is only known at cell centers, we must use some type of interpolation method to obtain the solution at mesh vertices. In [1], we assume that the solution at the small vicinity region surrounding the vertex varies linearly and use the simple least square method to determine the coefficients. Using this approach, the solution together with its derivatives can be obtained simultaneously. This approach works very well for well-shaped regular meshes. However, for high-aspect-ratio cells with large local surface curvature (Figure 1) where the reconstructed vertex lies outside the convex hull formed by its surrounding cell centers, we found that the simple method

DOI: 10.1002/fld

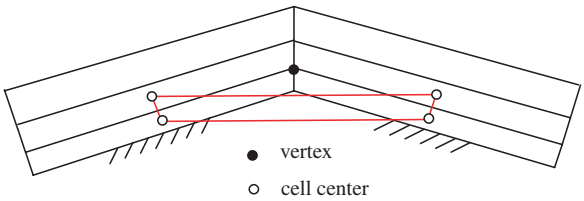

Figure 1. Illustration of high-aspect-ratio cells with surface curvature.

based on the inverse distance weighting is more robust:

$$u_v = \frac{\sum_{i=1}^{N} u_{c,i}/r_i}{\sum_{i=1}^{N} 1/r_i} \tag{2}$$

where $r_i = \sqrt{(x_i - x_c)^2 + (y_i - y_c)^2}$, the subscripts i and c stand for the vertex and the cell center, respectively, and N is the number of surrounding cells. The inverse distance averaging ensures that u_v will not exceed the range defined by solutions at its surrounding cell centers.

2.2. *Advection speed at faces*

To compute the inviscid (advection) flux when solving the momentum equations, we use the flux vector splitting technique to obtain the upwind flux. The flux vector is split according to the sign of the local advection speed across the cell interface, i.e.

$$\begin{aligned} \mathbf{F}_{\mathrm{INV}} &= \lambda_{ij}^{+}\mathbf{u}_{ij}^{\mathrm{L}} + \lambda_{ij}^{-}\mathbf{u}_{ij}^{\mathrm{R}} \\ \mathbf{u}_{ij}^{\mathrm{L}} &= \mathbf{u}_i + (\mathbf{x}_{ij} - \mathbf{x}_i)\cdot\nabla\mathbf{u}_i \\ \mathbf{u}_{ij}^{\mathrm{R}} &= \mathbf{u}_j + (\mathbf{x}_{ij} - \mathbf{x}_j)\cdot\nabla\mathbf{u}_j \end{aligned} \tag{3}$$

where the subscript 'ij' stands for the interface between cells 'i' and 'j', and 'L' and 'R' represent the left and the right states, respectively. The advection speed at the face $\lambda_{ij}^{\pm} = \frac{1}{2}(\lambda_{ij} \pm |\lambda_{ij}|)$ represents the positive and negative eigenvalues of the inviscid flux Jacobian matrix. A unique solution, $\mathbf{u}_{ij}$, at the cell interface must be obtained to evaluate $\lambda_{ij} = \mathbf{n}\cdot\mathbf{u}_{ij}$, which is the advection velocity normal to the interface. In [1], we use a sophisticated approach to compute $\mathbf{u}_{ij}$ for high accuracy. However, that approach causes the instability problem when the Reynolds number is high. This is an evidence showing that the upwind flux computed in such a way is not dissipative enough to suppress the instability. A common practice to increase the dissipation of the flux vector splitting scheme is to compute $\lambda_{ij}^{\pm}$ according to $\lambda_{ij}^{\pm} = \frac{1}{2}(\lambda_{ij} \pm \sqrt{\lambda_{ij}^2 + \varepsilon^2})$, where ε is a small number [14]. This modification of $\lambda_{ij}^{\pm}$ was proposed to correct the sonic glitch problem of the Steger–Warming scheme in compressible flows. This modification works somewhat in our incompressible solver. However, the addition of ε is unphysical and it is difficult to determine the magnitude of ε. Instead, we found that if $\mathbf{u}_{ij}$ is simply taken to be the arithmetic average of the interpolated velocities at vertices of faces, the scheme will be stabilized for flows at a high Reynolds number without sacrificing the accuracy. Recall that in Equation (1), u_k is obtained in the same way.

DOI: 10.1002/fld

By implementing the aforementioned two cures, our new hybrid scheme is able to simulate high Reynolds number laminar and turbulent flows. Note that we did not use any type of slope or flux limiters in the simulations that will be presented in Section 4.

3. IMPLEMENTATION OF THE SA-DES TURBULENCE MODEL

The SA-DES model [9] is derived from the SA one-equation eddy-viscosity RANS model. Non-dimensionalized by a set of reference values, u_{ref}, L_{ref} and v_{ref}, the one-equation SA-DES model can be expressed as

$$\frac{\partial \tilde{v}}{\partial t}+\mathbf{u}\cdot\nabla\tilde{v}=\frac{1}{\sigma Re}[\nabla\cdot((v+\tilde{v})\nabla\tilde{v})+c_{b2}|\nabla\tilde{v}|^2]+c_{b1}\tilde{S}\tilde{v}-\frac{c_{w1}f_w}{Re}\left(\frac{\tilde{v}}{d_{\text{DES}}}\right)^2 \tag{4}$$

where $\tilde{v}$ is the working variable in the order of the molecular viscosity v and Re is the Reynolds number. If the molecular viscosity is constant, then $v=1$ in Equation (4). In Equation (4), the second and the last term on the right-hand side are the production term and destruction term, respectively. The details of the SA-DES model can be found in [9].

3.1. Modifications for robustness

The functions in the SA-DES equation are very non-linear functions of $\tilde{v}$. Numerical experience shows that underflows and/or overflows of floating point values can easily happen if no care is taken. To improve the robustness of the DES model, we made some modifications of these functions shown in Equations (5)–(7). Figure 2 shows g vs. r, f_w vs. g and f_w vs. r, respectively:

$$f_{v1}=\begin{cases}0, & \chi\leqslant 2.5\times 10^{-5}\\ \dfrac{\chi^3}{\chi^3+c_{v1}^3} & \text{otherwise}\end{cases} \tag{5}$$

$$g=\begin{cases}250, & r\geqslant 3.0632301\\ r+c_{w2}(r^6-r), & 3.0632301>r\geqslant 0.005\\ (1-c_{w2})r, & r<0.005\end{cases} \tag{6}$$

$$f_w=\begin{cases}250\left[\dfrac{1+c_{w3}^6}{250^6+c_{w3}^6}\right]^{1/6}, & g\geqslant 250\\ g\left[\dfrac{1+c_{w3}^6}{g^6+c_{w3}^6}\right]^{1/6}, & 250>g\geqslant 0.005\\ \dfrac{g}{c_{w3}(1+c_{w3}^6)^{1/6}}, & g<0.005\end{cases} \tag{7}$$

DOI: 10.1002/fld

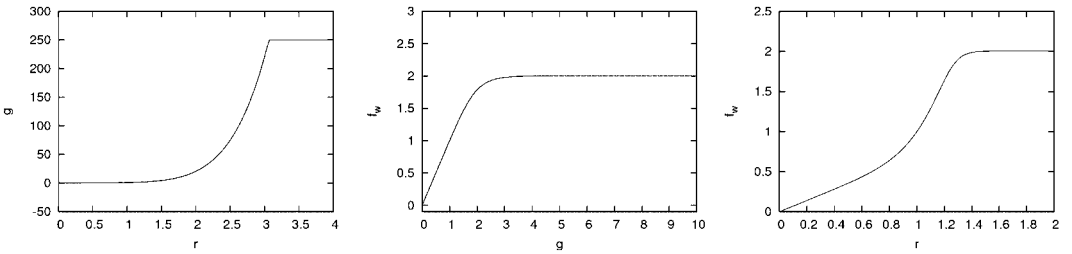

Figure 2. Functions used in the SA-DES turbulence model.

3.2. Mesh design guideline

The DES model combines the LES mode and the RANS mode in a unified formulation. In the LES mode, which is active in the separated region, the mesh is preferred to be isotropic. While in the RANS mode, which is activated in the attached boundary layer, the highly stretched cells are preferred to reduce the number of cells. Since the SA-DES model does not require any wall functions, the mesh close to the solid body surface must be carefully designed to accurately predict the aerodynamic/hydrodynamic forces. We follow the guideline in [15] to generate the high-aspect-ratio cells near the body. The first layer thickness is a function of the Reynolds number, i.e.

$$y^+ = 0.172 y^* Re^{0.9} \tag{8}$$

where $y^* = y/L$ is the non-dimensional first-layer thickness next to the body and L is the body length. Re is the flow Reynolds number based on the body length. $y^+ \approx 1$ is assumed in the first layer during the mesh generation stage. Therefore, according to Equation (8), the first-layer thickness of the mesh can be computed. Note that the actual y^+ value varies over the surface and depends on the local viscous flow solution.

4. NUMERICAL EXAMPLES

In this section, we first present some numerical results to demonstrate the performance of the current hybrid solver for high Reynolds number flows. Following those is a simple 3-D laminar case to show the 3-D capability of the current solver.

4.1. High Reynolds number over flat plate flow ($Re = 10^7$)

It is well known that the incompressible flow passing the smooth flat plate becomes turbulent when the Reynolds number exceeds 5×10^5. In this case, we chose the Reynolds number to be 10^7 to test the performance of the turbulence model. The mesh used in this simulation is shown in Figure 3. The thickness of the first layer adjacent to the flat plate is 2.9×10^{-6} leading to the maximum aspect ratio equal to 21 500. The mesh contains 9600 quadrilaterals. Figure 4 shows the computed friction coefficient distribution along the plate. Also shown on the same figure are the two empirical relations available in the literature [16]. Interestingly, the present results agree well with one of the empirical relation, i.e. Nikuradse's formulae. The solver converges well toward the steady state, which can be seen from the momentum residual convergence history (Figure 4).

DOI: 10.1002/fld

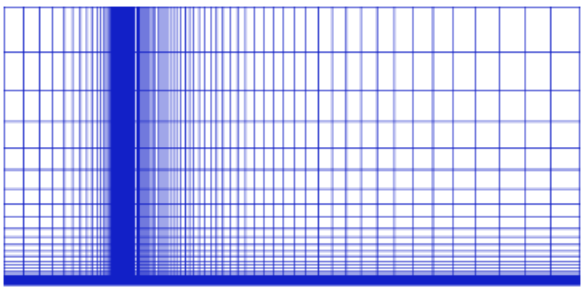

Figure 3. Mesh used in the flat plate simulation.

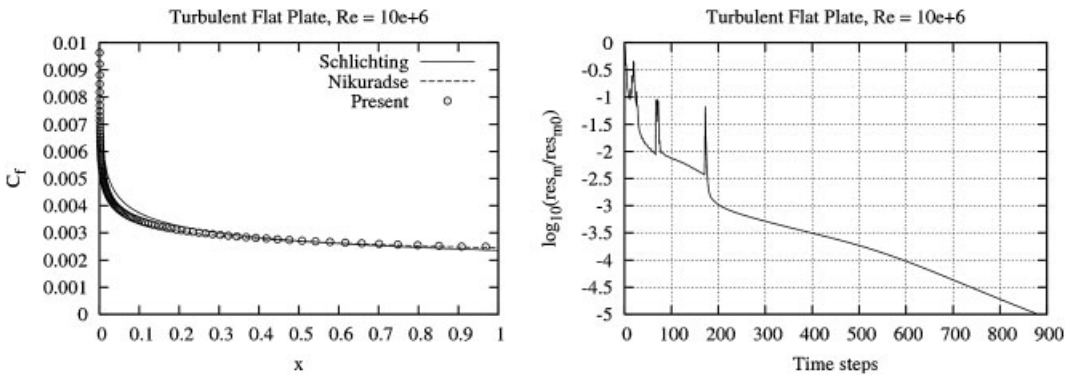

Figure 4. Friction coefficient distribution (left) and convergence history (right). Turbulent case.

To verify the accuracy of the baseline solver, we also run a laminar case with $Re = 2 \times 10^5$. The computed friction coefficient distribution is compared with the classic Blasius solution in Figure 5. Excellent agreement can be seen. On the basis of the results, we are quite confident about the accuracy of the current hybrid solver.

4.2. High Reynolds number flow around a high angle-of-attack NACA0015 airfoil ($Re = 1.5 \times 10^6, \alpha = 12°$)

This case is a more realistic example. The flight conditions are Mach $= 0.1235$, $Re = 1.5 \times 10^6$ and angle-of-attack $\alpha = 12°$. We assume that the flow is incompressible and use the present hybrid incompressible solver to simulate the flow. The mesh is a hybrid one containing 111 000 quadrilateral cells near the airfoil and 48 862 triangular cells elsewhere. There are 223 unevenly distributed points on the airfoil surface. The cell thickness of the first layer next to the airfoil is 10^{-5} times the chord length, which leads to the maximum aspect ratio of about 3000. The code was run in the unsteady mode even though a steady-state solution exists for this case. The time step is $\Delta t = 0.002$ and 7500 time steps have been run to reach the steady state. Figure 6 shows the near-field mesh and the computed pressure field. Figure 7 shows the computed pressure and friction coefficients on the airfoil surface. The role of the eddy viscosity is to postpone the flow separation and is

DOI: 10.1002/fld

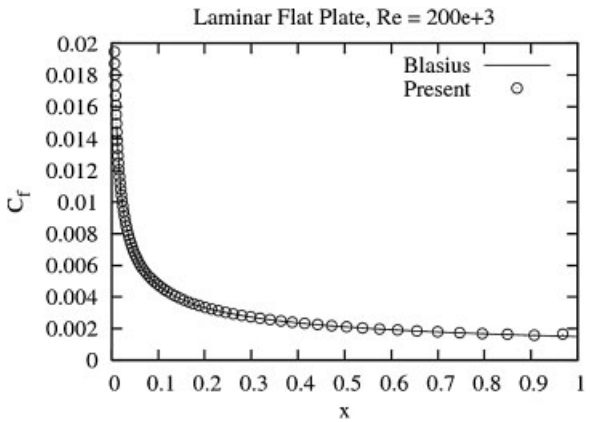

Figure 5. Friction coefficient distribution for the laminar case.

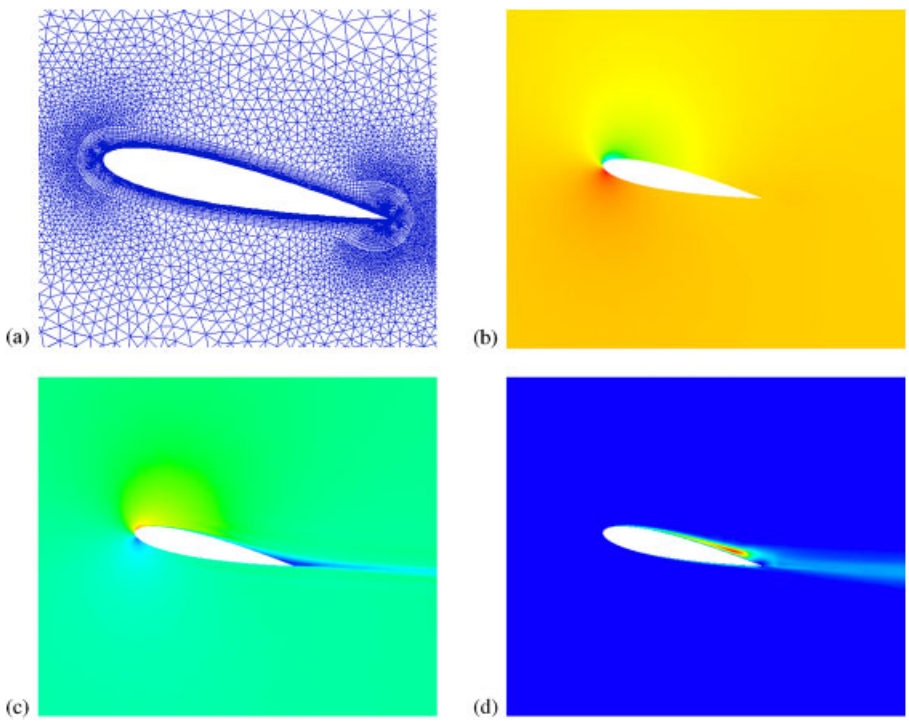

Figure 6. Near-field mesh and computed solution around the NACA0015 airfoil: (a) mesh near the airfoil; (b) pressure field; (c) velocity magnitude field; and (d) turbulent viscosity field.

essential for the correct prediction of the aerodynamic drag and lift. Figure 8 shows the drag and lift convergence histories. The time-averaged drag and lift are 0.02 and 1.075, respectively. Compared with the data provided in [17], we consider that the present results are fairly accurate.

DOI: 10.1002/fld

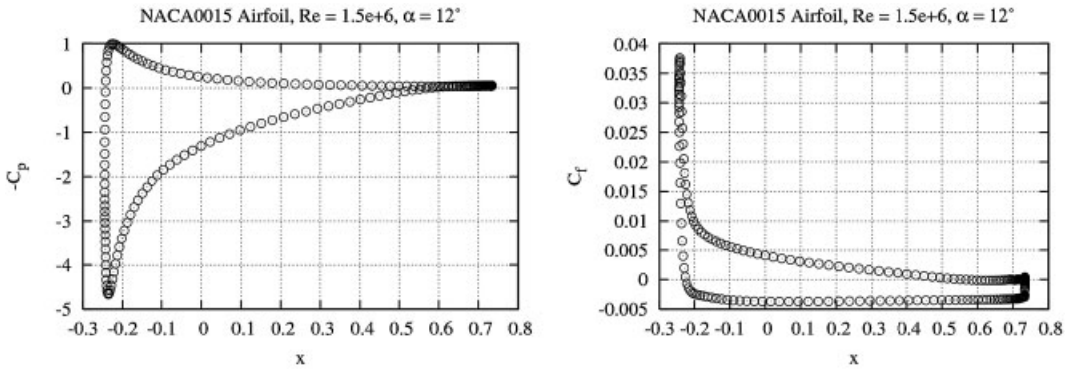

Figure 7. Computed pressure and friction coefficients on the NACA0015 airfoil surfaces.

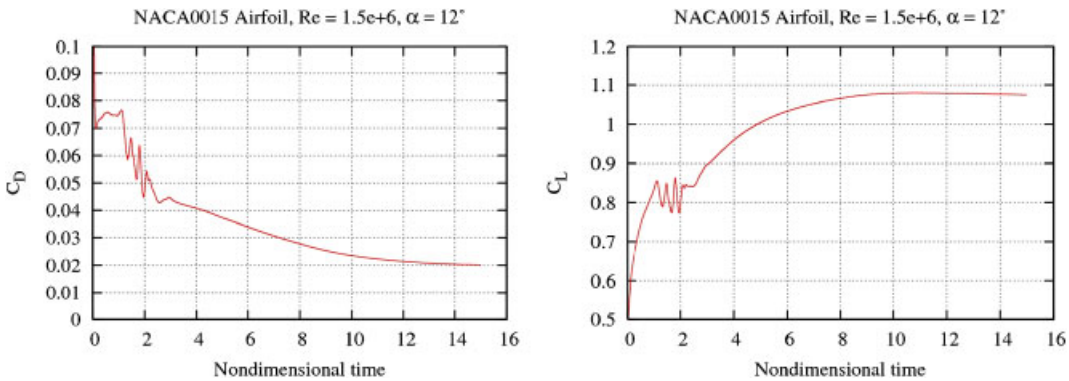

Figure 8. Convergence history of drag and lift coefficients on the NACA0015 airfoil surfaces.

We would like to take this example to demonstrate the efficiency of the current hybrid solver. Figure 9 is the convergence record of the momentum equation at the 200th time step taken from the real simulation. '`iit`' represents the outer Newton non-linear iterations. '`gmres iter#`' stands for the number of GMRES restarts. The integer before 'subiters' is the actual iterations (maximum limited by the specified size of the Krylov space) taken within each GMRES restart. We use the incomplete convergence in the GMRES solver in each Newton iteration. When the residual drops more than one order of magnitude, the GMRES is stopped and the next Newton iteration begins. When the total momentum residual has dropped more than three orders of magnitude, the solution is considered to have converged in this time step. As can be seen, 1 to 3 GMRES iterations are enough to reduce the residual one order of magnitude within each Newton iteration. This is a clear sign to show that the current LU-SGS preconditioner is very effective. Moreover, the outer Newton non-linear iterations converge well too. With four Newton iterations, the momentum residual drops 3.6 orders of magnitude. This effectiveness can be attributed in part to the accurate approximation of the Jacobian matrix. The 200th time step is at the quite early stage of the simulation. At a later stage toward the steady state, the convergence is even better. Figure 10 demonstrates a similar

DOI: 10.1002/fld

```
solving momentum equations..., reynolds =  1.50000E+06
iit =  1
   gmres iter#:  0 resid:  0.21504071E-01
   gmres iter#:  1 resid:  0.68724646E-03 after  1 subiters.
   gmres: convergence order =  1.495 iterno =    1
   |mom-res| = .62097E-04
iit =  2
   gmres iter#:  0 resid:  0.86991986E-03
   gmres iter#:  1 resid:  0.67842253E-04 after  1 subiters.
   gmres: convergence order =  1.108 iterno =    1
   |mom-res| = .25120E-05 order dropped:  1.393041
iit =  3
   gmres iter#:  0 resid:  0.81812087E-04
   gmres iter#:  1 resid:  0.43555104E-05 after  2 subiters.
   gmres: convergence order =  1.274 iterno =    2
   |mom-res| = .23625E-06 order dropped:  2.419703
iit =  4
   gmres iter#:  0 resid:  0.51983084E-05
   gmres iter#:  1 resid:  0.32152201E-06 after  3 subiters.
   gmres: convergence order =  1.209 iterno =    3
   |mom-res| = .15011E-07 order dropped:  3.616659
   converged. exiting sub-iteration.
```

Figure 9. Convergence of the momentum equation in a time step.

```
solving turbulence equation...
iit =  1
   gmres iter#:  0 resid:  0.16237973E+01
   gmres iter#:  1 resid:  0.41681197E-01 after  1 subiters.
   gmres: convergence order =  1.591 iterno =   1
   |turb-res| = .66312E-02
iit =  2
   gmres iter#:  0 resid:  0.41642035E-01
   gmres iter#:  1 resid:  0.76654733E-03 after  2 subiters.
   gmres: convergence order =  1.735 iterno =   2
   |turb-res| = .17006E-03 order dropped:  1.591000
iit =  3
   gmres iter#:  0 resid:  0.75023547E-03
   gmres iter#:  1 resid:  0.28837047E-04 after  2 subiters.
   gmres: convergence order =  1.415 iterno =   2
   |turb-res| = .30638E-05 order dropped:  3.335334
   converged. exiting sub-iteration.
```

Figure 10. Convergence of the turbulence equation in a time step.

convergence phenomenon for the turbulence equation in the same time step. It is clear that the stiff non-linear source terms in the turbulence equation did not cause any convergence problem. As for the convergence of the pressure Poisson equation, we need 825 iterations to drop five orders of magnitudes. We use the conjugate gradient solver with ILU(0) preconditioner for the pressure equation. Solving the pressure equation (1) is the most time-consuming task in the current code. The pressure solver consumed 75% of the total computational cost. The momentum equations and the turbulence equation consumed only 16 and 9%, respectively. We need to seek a more efficient pressure solver to reduce the overall cost.

DOI: 10.1002/fld

5. CONCLUSIONS

In this paper, we extend our hybrid unstructured FV/FE solver for incompressible Navier–Stokes flows at high Reynolds number. We first gave a brief overview of our baseline hybrid solver. We then provide two remedies to cure the deficiency of our solver when simulating the high Reynolds number flows where highly stretched cells exist. The one-equation Spalart–Allmaras Detached Eddy Simulation (SA-DES) turbulence model is incorporated into the solver to provide the turbulence viscosity. Some implementation issues are discussed to ensure the robustness of the turbulence model. Numerical results demonstrate the performance of the current solver for high Reynolds number flows. The resulting solver is stable and accurate for both laminar and turbulent flows. No slope or flux limiters are employed for all simulations presented here. In addition, the realistic simulation also showed the efficiency of the current solver, especially the LU-SGS preconditioners for the momentum equations and the turbulence equation.

A more efficient Poisson equation solver will be sought to improve the efficiency and reduce the overall computational cost.

ACKNOWLEDGEMENTS

Work is funded by Northrop Grumman Ship Systems and the National Science Foundation.

REFERENCES

1. Tu S, Aliabadi S. Development of a hybrid finite volume/element solver for incompressible flows on unstructured meshes. *International Journal for Numerical Methods in Fluids* 2007; **55**(2):177–203.
2. Guermond JL, Minev P, Shen J. An overview of projection methods for incompressible flows. *Computer Methods in Applied Mechanics and Engineering* 2006; **195**:6011–6045.
3. Timmermans LJP, Minev PD, van de Vosse FN. An approximate projection scheme for incompressible flow using spectral elements. *International Journal for Numerical Methods in Fluids* 1996; **22**:673–688.
4. Aliabadi S, Johnson AA, Abedi J. Stabilized-finite-element/interface-capturing technique for parallel computation of unsteady flows with interfaces. *Computers and Fluids* 2003; **32**:535–545.
5. Aliabadi S, Tu S, Watts MD, Ji A, Johnson AA. Integrated high performance computational tools for simulations of transport and diffusion of contaminants in urban areas. *International Journal of Computational Fluid Dynamics* 2006; **20**(3–4):253–267.
6. Delanaye M. Polynomial reconstruction finite volume schemes for the compressible Euler and Navier–Stokes equations on unstructured adaptive grids. *Ph.D. Thesis*, Universite de Liege, 1996.
7. Tu S, Watts MD, Fuller A, Patel R, Aliabadi S. Development and performance of *CaMEL_Aero*, a truly matrix-free, parallel and vectorized unstructured finite volume solver for compressible flows. *Proceedings of the 25th Army Science Conference*, Orlando, FL, 2006.
8. Spalart PR, Jou W-H, Strelets M, Allmaras SR. Comments on the feasibility of LES for wings and on hybrid RANS/LES approach. *Proceedings of the 1st AFOSR International Conference on DNS/LES*, Columbus, OH, 1997.
9. Nikitin NV, Nicoud F, Wasistho B, Squires KD, Spalart PR. An approach to wall modeling in large-eddy simulations. *Physics of Fluids* 2000; **12**(7):1629–1632.
10. Strelets M. Detached eddy simulation of massively separated flows. *The 39th AIAA Aerospace Sciences Meeting and Exhibits*, Reno, NV, AIAA Paper 2001-0879, 2001.
11. Scott AM, Matthew BS, Russell MC, James RF. DES grid resolution issues for vortical flows on a Delta wing and an F-18C. *The 41st Aerospace Sciences Meeting & Exhibit*, Reno, NV, AIAA Paper 2003-1103, 2003.
12. Kapadia S, Roy S, Wurtzler K. Detached eddy simulation over a reference Ahmed car model. *The 41st Aerospace Sciences Meeting and Exhibit*, Reno, NV, AIAA Paper 2003-0857, 2003.
13. Forsythe JR, Hoffmann KA, Cummings RM, Squires KD. Detached eddy simulation with compressibility corrections applied to a supersonic axisymmetric base flow. *Journal of Fluids Engineering* 2002; **124**(4):911–923.

DOI: 10.1002/fld

14. Burning PG, Steger JL. Solution of the two-dimensional Euler equations with generalized coordinate transformations using flux vector splitting. *AIAA Paper 82-0971*, Reno, NV, 1982.
15. Lin C-W, Percival S, Gotimer EH. Viscous drag calculations for ship hull geometry. *The 9th International Conference on Numerical Methods in Laminar and Turbulent Flow*, Atlanta, GA, 1995.
16. Schlichting H. *Boundary Layer Theory* (7th edn). McGraw-Hill: New York, 1996.
17. Sheldahl RE, Klimas PC. Aerodynamic characteristics of seven symmetrical airfoil sections through 180-degree angle of attack for use in aerodynamic analysis of vertical axis wind turbines. *Sandia National Laboratories Report SAND80-2114*, 1981.

DOI: 10.1002/fld